# *Articles*

## Electronic Structure of Intercalation Compounds of $Co_xNbS_2$

Masanobu Nakayama,[†] Kazumoto Miwa,[†] Hiromasa Ikuta,[‡] Hirofumi Hinode,[§] and Masataka Wakihara*,[†]

*Department of Applied Chemistry, Tokyo Institute of Technology, Ookayama, Meguro-ku, Tokyo 152-8552, Japan, Faculty of Symbolic System Science, Fukushima University, Kanayagawa, Fukushima-shi, Fukushima 960-1296, Japan, and Department of International Development Engineering, Tokyo Institute of Technology, Ookayama, Meguro-ku, Tokyo 152-8552, Japan*

*Received April 22, 2006. Revised Manuscript Received August 9, 2006*

Cobalt intercalation into niobium disulfide with layered structure is presented. Powder X-ray diffraction study reveals that single-phase $Co_xNbS_2$ forms in the compositional range of $0.15 \leq x \leq 0.55$. The hexagonal lattice parameters *a* and *c* monotonically increase with cobalt content up to $x \sim 0.5$, while *a* and *c* are constant and decreasing from $x = 0.5$ to 0.55, respectively. The temperature dependence of electric resistivity shows metallic behavior at $0.15 \leq x < 0.49$ whereas semiconducting behavior is seen at $0.49 \leq x \leq 0.55$, so that metal−semiconductor transition occurs at the composition $x = 0.49$. The temperature dependence of magnetic susceptibility obeys a Curie−Weiss law in the whole compositional range, suggesting localized electronic behavior around Co ions. The valance state of Co in $Co_xNbS_2$ was evaluated as divalent from effective Bohr magneton. The ab initio computation based on density functional theory was performed for $NbS_2$ and $Co_{1/3}NbS_2$. The $d_{z2}$ band arising from the $NbS_6$ trigonal-prism crystal field was formed and half-filled with electrons in $NbS_2$. Electrons were injected into this $d_{z2}$ band by $Co^{2+}$ intercalation, and the band would be filled with electrons at the composition $x \sim 0.49$, causing metal−semiconductor transition.

### Introduction

Topochemical insertion, or intercalation, of various kinds of metals into transition-metal oxides and sulfides has been explored extensively in the context of developing battery and electrochromic devices.[1−4] However, material with metal insertion sites is attractive enough not only to be used for the practical purpose as above but also to be employed as a model material in the fundamental study in solid-state science. For example, the intercalation of alkali atoms in layered type sulfides, $MoS_2$ or $ZrSe_2$, converts their semiconductive nature into metallic and superconductivity at low temperatures.[5,6] Thus, intercalation is particularly significant in the modification of materials' properties.

Niobium disulfide $NbS_2$ has been examined because of characteristic optical[7,8] and magnetic properties[9−11] and superconductive behavior.[9,12,13] The structure of $NbS_2$ belongs to a hexagonal system, and the S−Nb−S sandwich layers pile along the *c* axis.[7] Transition metals such as Ti, V, Cr, Mn, Fe, Co, and Ni can intercalate into the octahedral vacancies of the van der Waals gaps of $NbS_2$ (Figure 1). However, such intercalation compounds, $M_xNbS_2$, have been reported only for the limited compositions *x*, such as $x = 1/2$, 1/3, and 1/4, and little information has been available on the

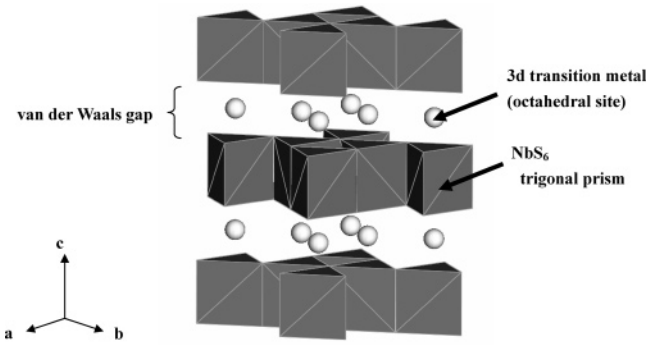


**Figure 1.** Typical crystal structure of 3d transition metal intercalation niobium sufides, $M_xNbS_2$.

* Corresponding author: Tel.: + 81 3 5734 2145; Fax: +81 3 5734 2146.
[†] Department of Applied Chemistry, Tokyo Institute of Technology.
[‡] Fukushima University.
[§] Department of International Development Engineering, Tokyo Institute of Technology.

(1) Thackeray, M. M. *Prog. Solid State Chem.* **1997**, *25*, 1.
(2) Tarascon, J. M.; Armand, M. *Nature* **2001**, *414*, 359.
(3) Monk, P. M. S. *Crit. Rev. Solid State Mater. Sci.* **1999**, *24*, 193.
(4) Granqvist, C. G. *Electrochim. Acta.* **1999**, *44*, 3005.
(5) Woollam, J. A.; Somoano, R. B. *Phys. Rev. B* **1976**, *13*, 3843.
(6) Onuki, Y.; Inada, R.; Tamura, S.; Yamanaka, S.; Kamimura, H. *Synth. Met.* **1983**, *5*, 245.
(7) Wilson, J. A.; Yoffe, A. D. *Adv. Phys.* **1969**, *18*, 193.
(8) Li, Z. M.; Bergersen, B.; Palffy-Muhoray, P.; Beigie, D. *Can. J. Phys.* **1988**, *66*, 228.
(9) Fisher, W. G.; Sienko, M. J. *Inorg. Chem.* **1980**, *19*, 39.
(10) Hulliger, F.; Pobitschka, E. *J. Solid State Chem.* **1970**, *1*, 117.
(11) van den Berg, J. M.; Cossee, P. *Inorg. Chim. Acta* **1968**, *2*, 143.
(12) Ikebe, M.; Muto, Y. *Synth. Met.* **1983**, *5*, 229.
(13) Jellinek, F. *Ark. Kemi.* **1963**, *20*, 447.

10.1021/cm060932n CCC: $33.50 
Published on Web 09/22/2006

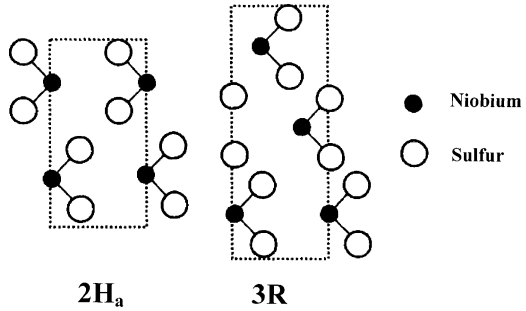


**Figure 2.** Schematic figures for polytypes of $NbS_2$ with (1120) section

single-phase region, or on the compositional dependence of physical properties of $M_xNbS_2$.[14]

In this paper, we synthesized and investigated the electric resistivity and magnetic susceptibility of $Co_xNbS_2$ as a function of cobalt content and temperature. In addition, ab initio study based on density functional theory (DFT) was carried out to understand their physical properties from the viewpoint of electronic structure.

## Experimental Section

The intercalation compounds $Co_xNbS_2$ were synthesized by mixing Co powder (99.98%, Soekawa Chem. Co. Ltd.), Nb powder (99.9%, Soekawa Chem. Co. Ltd.), and crystalline S (99.9999% Wako Chem. Co. Ltd.). They were mixed with a desired ratio, pressed into a pellet, and sealed in an evacuated quartz ampule. The pellet was heated first at 400 °C for 1 day and then at 1000 °C for 4 days. The obtained samples were ground, sealed again, heated at 1000 °C for 4 days, and quenched in ice−water. The phase identification and the evaluation of the lattice parameters of the samples were carried out by powder X-ray diffraction using Cu Kα radiation.

The electrical resistivity measurement on the pellet sample was performed using the standard dc four-probe technique under $H_2$ atmosphere in the temperature range 80−300 K. The magnetic susceptibilities were measured using the SQUID method (Quantum Design MPMS-5A) in the temperature range 4.5−300 K under the static field of 1000 G.

## Results and Discussion

Figure 2 displays the schematic figures of two known polytype structures for $NbS_2$, 2H$_a$ and 3R. In both structures, $NbS_2$ layers with trigonal prismatic symmetry and van der Waals gap stack alternatively, and 3d metal ions intercalate into octahedral vacancies of the van der Waals gap (see also Figure 1). All the powder XRD patterns of the samples $Co_xNbS_2$ in the range of $0.15 \leq x \leq 0.55$ were indexed on hexagonal unit cell of 2H$_a$ (Figure 3). Yellow colored elemental sulfur was deposited at $x < 0.15$ in the ampule, while unknown peaks appeared in $x > 0.55$. Thus, the single-phase region of $Co_xNbS_2$ under the present synthesis conditions was determined to be in the range of $0.15 \leq x \leq 0.55$. Herein, we will use nominal composition, since no sulfur deposition was detected by XRD in this regime. In detail, additional peaks were observed at $2\theta \sim 20°$ around the composition $x = 1/3$, ascribing to the formation of $\sqrt{3}\, a_0 \times \sqrt{3}\, a_0$ superstructure (see Figure 4) caused by the ordered arrangement of Co ions. ($a_0$ refers to the lattice parameter of the hexagonal basal plane of the host crystal.)

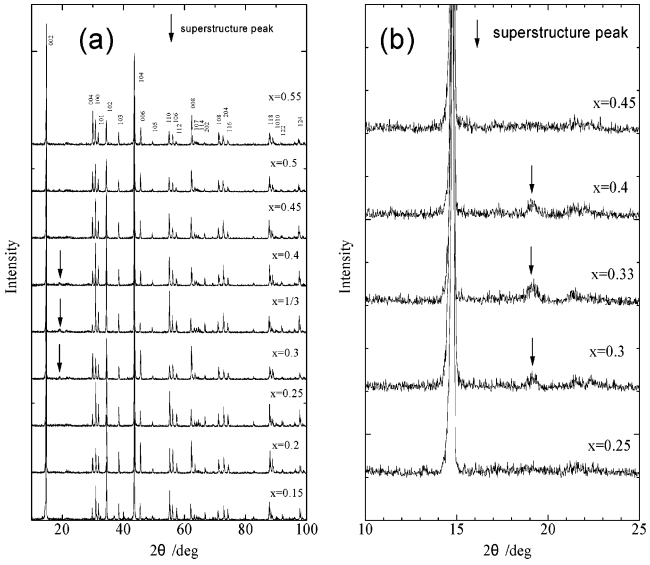


**Figure 3.** (a) Powder X-ray diffraction patterns of $Co_xNbS_2$. (b) Magnification of superstructure peaks.

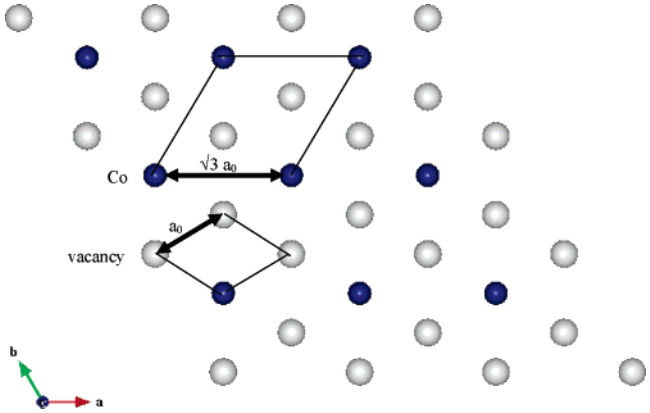


**Figure 4.** Co arrangement in $\sqrt{3}\, a_0$ x $\sqrt{3}\, a_0$ superstructure for $Co_{1/3}NbS_2$. The darker circle and the brighter one indicate Co and vacancy, respectively. The $a_0$ refers the lattice parameter of the hexagonal basal plane of the host crystal.

Variation of the hexagonal lattice parameters were presented as a function of Co content $x$ in Figure 5. In the region of $0.15 \leq x \leq 0.5$, the lattice parameters $a$ and $c$ monotonically increased with Co intercalation. The elongation of the $c$ axis (∼0.8%) suggests that intercalated Co expands the van der Waals gaps. However, this tendency changed beyond $x \sim 0.5$; the lattice parameter $a$ kept constant, while the lattice parameter $c$ was decreased with composition $x$.

Figure 6 shows the temperature dependence of the electric resistivity in the range from 90 to 300 K. Note that sintered polycrystalline sample was used in this measurement, so that the anisotropic effect of the lattice (e.g. in-plane and intra-plane conduction) and the grain boundary contribution to the electronic resistivity are not separated. The samples with composition $0.15 \leq x \leq 0.48$ show increase in resistivity with temperature, indicating metallic behavior. On the other hand, the resistivity decreased with temperature in region $x \geq 0.49$, which relates to the semiconductive behavior. Therefore, metal−semiconductor transition took place when

(14) Parkin, S. S. P.; Marseglia, E. A.; Brown, P. J. *J. Phys. C: Solid State Phys.* **1983**, *16*, 2765.

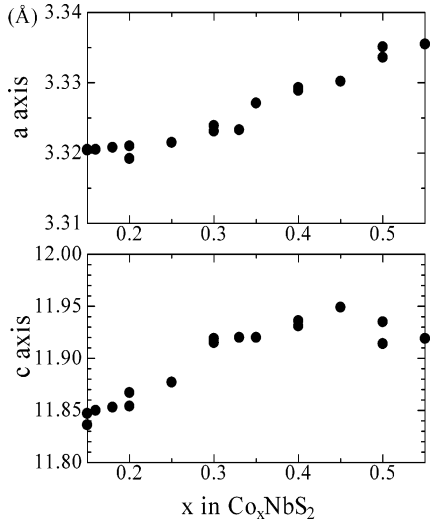


**Figure 5.** Variation of the hexagonal lattice parameters as a function of composition $x$ in $Co_xNbS_2$; all the error bars for observed lattice parameters are too small to show up.

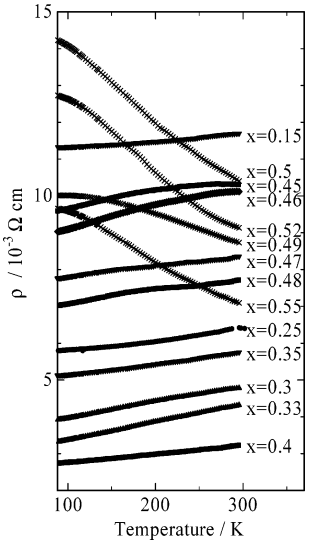


**Figure 6.** Variation of the electrical resistivity as a function of temperature. The solid dot and cross indicate metallic and semiconductive behavior, respectively.

the composition was between $x = 0.48$ and 0.49. It is known that the formation of the half filled $d_{z2}$ band in $NbS_2$ is due to the crystal field of trigonal prism symmetry (we will show this validity later using ab initio computation). Thus, the sample would show metallic behavior before filling of $d_{z2}$ band. In this simple viewpoint, the $d_{z2}$ band would be filled at $x = 0.5$ where metal−semiconductor transition was observed. The valence state of cobalt is expected to be +2, since the unoccupied $d_{z2}$ band can accommodate one electron. This is verified in the results of the magnetic susceptibility measurements mentioned later. (The small deviation in transition composition between experimental ($x \sim 0.48$) and theoretical one ($x = 0.5$) would be due to stoichiometric error. Although we assumed nominal composition in this paper, small sulfur deposition might occur. However, sulfur deficiency, or $\delta$ in $Co_xNbS_{2-\delta}$, would be quite small ($\delta < 0.02$) judging from metal−semiconductor transition composition.) Figure 7 shows the compositional dependence of electric resistivity at room temperature (298 K). Solid and

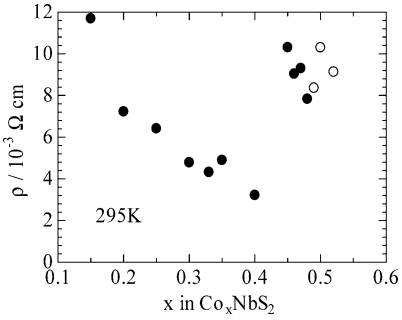


**Figure 7.** Variation of the electrical resistivity at 295 K versus composition $x$ in $Co_xNbS_2$. Solid and open circles indicate metallic and semiconductive behavior, respectively.

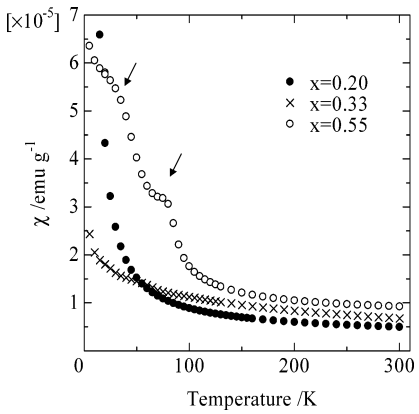


**Figure 8.** Typical examples of variation of the magnetic susceptibility with temperature for $Co_xNbS_2$.

open symbols indicate metallic and semiconductive materials, respectively. The resistivity decreased linearly as $x$ increased in the range of $0.15 \leq x \leq 0.45$. Maybe this stems from the increase of carrier mobility in the $d_{z2}$ band, because total carrier density $n_e \times n_h$ decreased in this regime. ($n_e$ and $n_h$ indicate the number of electrons and holes, respectively). A sudden increase in electric resistivity indicated around $x \sim 0.45$, which maybe originates from the filling of the $d_{z2}$ band, causes an increase in the effective mass of electrons. In addition, the composition where electric resistivity humped matches the one where the changes in the dependence of lattice parameter $c$ are observed (see Figure 3). Thus, the electronic resistivity may relate to the structural modification during Co intercalation.

Figure 8 shows the typical examples of temperature dependence of magnetic susceptibility. In all the samples, the magnetic susceptibility behavior obeyed a Curie−Weiss law described by

$$\chi = \chi_0 + \frac{C_{mol}}{T - \theta}$$

where $\chi_0$ is a temperature-independent term, $C_{mol}$ a molar Curie constant, and $\theta$ a Weiss temperature. The sample with a higher amount of Co ions shows humps or a bend around 40 and 90 K in the curves of magnetic susceptibility (see arrow in Figure 8). Although the exact reason is uncertain, several reasons could be suggested: (1) impurity oxygen,[15]

(15) Yan, J.; Ramamujachary, K. V.; Greenblatt, M. *Mater. Res. Bull.* **1995**, *30*, 463.

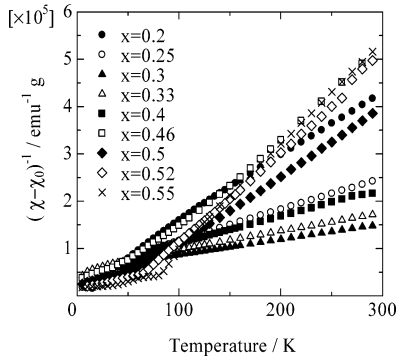


**Figure 9.** Inverse magnetic susceptibility versus temperature for $Co_xNbS_2$.

**Table 1. Magnetic Parameters of $Co_xNbS_2$**

| x in $Co_xNbS_2$ | $\theta$/K | $P_{eff}/\mu_B$ per Co | $S/\mu_B$ per Co |
|---|---|---|---|
| 0.20 | −25.9 | 2.26 | 0.74 |
| 0.25 | −97.5 | 2.29 | 0.75 |
| 0.30 | −167.0 | 3.78 | 1.46 |
| 0.33 | −155.0 | 3.33 | 1.24 |
| 0.40 | −36.6 | 1.85 | 0.64 |
| 0.46 | −7.6 | 1.60 | 0.44 |
| 0.50 | 8.6 | 1.60 | 0.44 |
| 0.52 | 15.4 | 1.48 | 0.39 |
| 0.55 | 52.6 | 1.13 | 0.35 |

(2) Hall effect,[16] (3) spin-glass behavior,[17] and so on. Since these abnormal changes in magnetic susceptibility depended strongly on the Co contents, formation of spin glass is most likely to occur in this system. This spin-glass is only observed for the sample with semiconductive behavior, so that this does not stem from RKKY interaction but rather from but frustration between Co 3d localized spin arising from triangle cluster formation. The relationship between temperature and inverse magnetic susceptibility is shown in Figure 9. The values of $C_{mol}$ and $\theta$ were obtained by a least squares refinement and summarized in Table 1. Note that accurate estimation is difficult due to their small values of $\chi_0$ on the order of $10^{-6}$ emu $g^{-1}$.

Although the metallic behavior was observed at $0.15 \leq x < 0.49$ in electric resistivity measurement, the localized electronic configuration is indicated from the Curie−Weiss manner of magnetic susceptibility. As discussed above, $NbS_2$ forms wide band structure and their electrons are delocalized, showing such as Pauli paramagnetism which contributes to the temperature-independent term of $\chi_0$. One can expect that Kondo or RKKY interaction comes from the interaction between free and localized electrons in metallic conduction phase. However, no marked changes in Weiss temperature were observed at metal−insulater transition composition (discussed later in Figure 11). Thus, we infer that the Kondo or RKKY interaction is of small importance in this system. Therefore, the localized nature of electrons mainly stems from the intercalated Co ions. To estimate the valence state of Co ions, an effective Bohr magneton $P_{eff}$ and spin quantum number $S$ per Co ions were calculated using the value of $C_{mol}$ and listed in Table 1, and $S$ is plotted in Figure 10. For

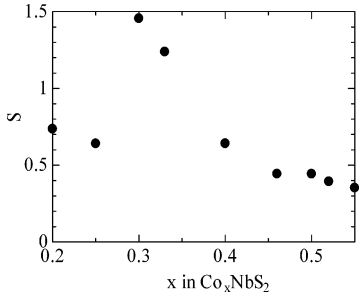


**Figure 10.** Variation of the estimated spin quantum number $S$ as a function of composition $x$ in $Co_xNbS_2$.

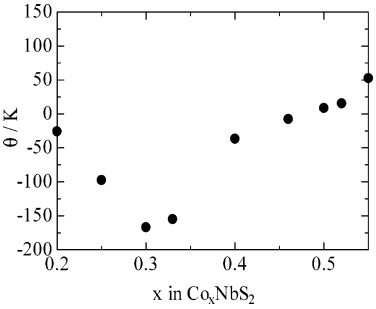


**Figure 11.** Variation of the estimated Weiss temperature $\theta$ as a function of composition $x$ in $Co_xNbS_2$.

the estimation of $S$, it was assumed that only spins contribute to $C_{mol}$. Except for the samples with $x = 0.3$ and $x = 1/3$, the values of $S$ were about 0.5, which corresponds to $Co^{2+}$ with low-spin electronic configuration. On the other hand, the high-spin configuration for $Co^{2+}$ was indicated at the compositions of $x = 0.3$ and 1/3, where the values of $S$ were about 1.5. Accordingly, the cobalt ions intercalated into layered $NbS_2$ structure with the oxidation state of +2, and low-spin to high-spin phase transition was around $x = 1/3$. Although the reason for this transition is uncertain, it would relate to the superstructure formation around $x = 1/3$. Usually, long-range ordering of the lattice does not affect the high and/or low spin configuration. However, we infer that the superlattice formation leads to the anomaly changes in the crystal field. One can see that the lattice parameter $c$ increased linearly with composition $x$, however, it humped slightly at the superlattice region. Since the $e_g$ electrons are directly linked to the S 3p orbital, the increase in lattice parameter $c$ would reduce electron−electron repulsive interaction. This effect would make the high spin configuration to be stable. In addition, all the Co ions are surrounded by vacancies in intercalated site, when superlattice forms. (Figure.4) Thus, the short-range exchange interaction between the Co ions is expected to disappear for the samples around $x = 1/3$. Further study is needed to understand the high-low spin transition around $x = 1/3$.

Figure 11 shows the plots of Weiss temperature $\theta$ as the function of composition $x$. The sudden decrease of the $\theta$ was observed at the composition $x = 0.3$ and 1/3, corresponding to the formation of superstructure and high-spin configuration. Maybe, the direct exchange interaction between Co ions would be depressed as mentioned above, while superexchange interaction works instead in this region. The low-spin to high-spin transition of $Co^{2+}$ increases the $e_g$ electrons which directly link to the anion S orbital. This would lead

(16) Nozaki, H.; Saeki, M.; Onoda, M. *J. Solid State Chem.* **1995**, *116*, 392.
(17) Matsuura, K.; Wada, T.; Nakamizo, T.; Yamauchi, H.; Tanaka, S. *J. Solid State Chem.* **1991**, *94*, 294.

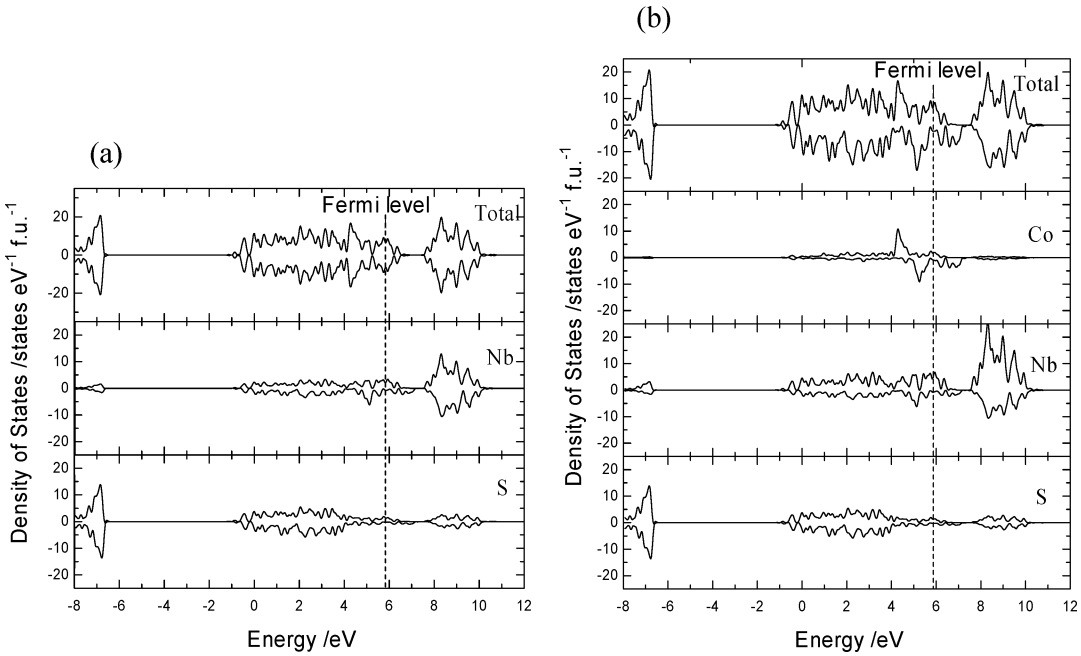


**Figure 12.** DOS for (a) $NbS_2$ and (b) $Co_{1/3}NbS_2$.

**Table 2. Comparison Hexagonal Lattice Parameters between Optimized Values by Computation and Measured Values by Experiment**

| | computation[a] | experiment |
|---|---|---|
| $NbS_2$ | $a = \sqrt{3}\, a_0 = 5.7566$<br>$c = 11.8667$ | |
| $Co_{1/3}NbS_2$ | $a = \sqrt{3}\, a_0 = 5.7822$<br>$c = 11.6894$ | $a = \sqrt{3}\, a_0 = 5.7561$<br>$c = 11.920$ |

[a] In the computation, the superlattice was used with $\sqrt{3}\, a_0 \times \sqrt{3}\, a_0$.

to the enhancement of the antiferromagnetic superexchange interaction. Thus, the Weiss temperature decreased at the composition $x = 0.3$ and 1/3. Except for this superstructure region, the $\theta$ gradually increased with composition $x$. The sign of $\theta$ is changed from negative to positive at $x = 0$, indicating the magnetic interactions changed from antiferromagnetic to ferromagnetic. This may originate from the increase of exchange interactions between Co and neighboring Co.

To understand the above experimental observations, ab initio computation based on density functional theory (DFT) was carried out for $NbS_2$ and $Co_{1/3}NbS_2$. The structure model reported by Parkin et al.[14] was used for $Co_{1/3}NbS_2$ as an initial structure. On the other hand, Co was simply removed from the structure for the computation of $NbS_2$. Vienna ab initio simulation package (VASP)[18] was utilized with generalized gradient approximation (GGA) and with the projector-augmented wave (PAW) method.[19,20] Antiferromagnetic arrangement was applied as indicated in magnetic susceptibility measurement for $Co_{1/3}NbS_2$. Relaxation was allowed, and the final energies of the optimized geometries were recalculated so as to correct changes in the plane-wave basis during relaxation. Table 2 summarizes the lattice parameters for optimized structure and experimental results, showing each deviation is less than 2% for $Co_{1/3}NbS_2$. Figure 12 represents the total and partial density of state obtained by ab initio computation. In $NbS_2$ (Figure 12a), partial DOS of sulfur forms a wide valence band from $-2$ to 4 eV, whereas that of niobium split into a $d_{z2}$ band and a remaining 4d electron band, residing around 5 eV and from 7 to 9 eV, respectively. As seen in Figure 12, the shape of both sulfur and niobium bands are similar, indicating strong hybridization between Nb 4d and S 3p levels. The Fermi level is placed at the center of Nb $d_{z2}$ band, so that metallic conduction via the Nb $d_{z2}$ band is predicted in $NbS_2$. The partial DOS of sulfur and niobium for $Co_{1/3}NbS_2$ (Figure 11b) almost maintained that for $NbS_2$. Hence, the rigid band model of $NbS_2$[21] could be supported for the $Co_xNbS_2$ system. The Co 3d band placed from 4 to 7 eV where the Nb $d_{z2}$ band resided, indicating that electrons of intercalated Co ions are injected into the Nb $d_{z2}$ band. As discussed before, the $d_{z2}$ band would be filled with one electron injection, which corresponds to the intercalation of 1/2 mol $Co^{2+}$ in the $NbS_2$ structure. Therefore, the metal−semiconductor transition occurred at the composition $x = 0.5$ in $Co_xNbS_2$. In detail, the Co 3d band split into $t_{2g}$ and $e_g$ bands due to octahedral symmetry and formed sharper and narrower band structure than that of the Nb 4d and S 3p bands. No marked hybridization was indicated between Co 3d and S 3p bands. Thus, 3d electrons of Co caused localized magnetic behavior, such as Curie−Weiss behavior around room temperature. Accordingly, ab initio computation supports well the observed electric resistivity and magnetic susceptibility behavior.

## Conclusions

(1) Single phase $Co_xNbS_2$ was synthesized in the compositional range of $0.15 \le x \le 0.55$. Superstructure with $\sqrt{3}a_0$

(18) Kresse, G.; Furthmuller, J. *Phys. Rev. B* **1999**, *54*, 11169.
(19) Blöchl, P. E. *Phys. Rev. B* **1994**, *50*, 17953.
(20) Kresse, G.; Joubert, D. *Phys. Rev. B* **1999**, *59*, 1758.
(21) Friend, R. H.; Yoffe, A. D. *Adv. Phys.* **1987**, *36*, 1.

$\times \sqrt{3}a_0$ was formed around $x = 1/3$ due to ordering of intercalated Co arrangement.

(2) Electric resistivity measurement reveals the metal−semiconductor transition at $x = 0.49$ arising from filling of the $d_{z2}$ orbital.

(3) Magnetic susceptibility follows a Curie−Weiss law and indicates that the valence state of Co is +2. The changes in spin configuration are observed and related to the arrangement of Co ions. High spin configuration is observed in the superstructure region, while low spin configuration is formed in the remaining region.

**Acknowledgment.** This work is supported by The Thermal & Electric Energy Technology Foundation in Japan. We express sincere gratitude to Prof. Hidekazu Tanaka (Tokyo Institute of Technology) for fruitful discussion.

CM060932N